UAV PATH FOLLOWING FOR CONSTANT LINE-OF-SIGHT

Rolf Rysdyk, * *University of Washington, Seattle, WA 98195*

ABSTRACT

This work provides algorithms for flight path guidance and synchronous camera angles to observe a target. The observation of the target is affected by the environment, maximum aircraft performance, and camera limits. Analytic expressions are derived for trajectories required for constant line-of-sight orientation relative to the aircraft. A guidance law based on 'good helmsman' behavior is implemented. An observer is used to estimate wind data, which is used to orient the trajectories about the target. Results are demonstrated in simulated maneuvers with exposure to variable wind and turbulence.

1. NOMENCLATURE

Symbols

a	sensitivity parameter for ground track convergence
$c_{(\cdot)}$	$\cos(\cdot)$
d	distance
g	gravity constant
x	position along x-axis
y	position along y-axis
z	position along z-axis
R	Radius
s	arclength position along desired path
$s_{(\cdot)}$	$\sin(\cdot)$
$\mathcal{F}_b$	'body-fixed' frame
$\mathcal{F}_s$	Serret-Frenet frame, see Fig(1)
$t_{(\cdot)}$	$\tan(\cdot)$
$\mathbf{V}$	Velocity
V_a	Airspeed
V_c	Groundspeed, inertial speed
V_w	Windspeed (inertial)
$\mathbf{x}_b, \mathbf{y}_b, \mathbf{z}_b$	body-fixed axes system
α	Angle of attack
β	Angle of side slip
y_s	Normal distance, course deviation, or cross-track error
$\kappa(s)$	Curvature of desired path at position s
κ	Camera tilt-angle
λ	Camera pan-angle
ϕ	Bank angle
ρ	Density
χ	Course
ψ	Heading
ψ_p	'Clock angle' relative to target (Bearing of aircraft from the target)
ζ	Bearing angle of target from the aircraft

Subscripts

ac	Aircraft center of gravity
b	Body-fixed reference frame
c	Inertial or Command
e	Earth reference frame (assumed as the 'inertial frame')
$icpt$	Intercept
m	Measured
tgt	Target
w	Wind

Superscripts

$\hat{\cdot}$	Normalized
$\tilde{\cdot}$	Error relative to desired path
$\vec{\cdot}$	Directed vector quantity

2. INTRODUCTION

The objective of this work is to provide algorithms for flight path guidance and synchronous camera angles to observe a target [1]. The observations may be affected by sunlight angles, maximum aircraft performance, and camera limits; pan angle, tilt angle, and zoom [2]. In this work trajectories are proposed and a guidance law is designed that results in **constant line-of-sight orientation** relative to the aircraft. This terminology is not to be confused with 'line-of-sight guidance' algorithms [3] which refers to a method to model 'helmsman behavior'.

The UAV control problem typically involves: airspeed, aerodynamic side-slip angle, turn rate, and flight-path angle. With most conventional aircraft these degrees of freedom are controlled with aerodynamic control surfaces (ailerons, elevator, and rudder) about three body axes, and the propulsion source (throttle). The aircraft under consideration includes altitude and airspeed hold functions using throttle and elevator, and automatic turn coordination using rudder. This leaves the ailerons to address the course deviation problem. The ailerons control the aircraft roll degree of freedom and hence the bank angle. For design of the guidance element, the aircraft bank-angle may be considered as the control

*Assistant Professor, Department of Aeronautics and Astronautics, email: rysdyk@aa.washington.edu

variable. The bank angle in a steady state coordinated turn is kinematically related to the heading rate of turn. The course deviation problem consists of stabilizing two degrees of freedom to zero: course angle error, and cross track distance. Hence, this provides the non-trivial design problem of controlling motion of an under-actuated vehicle. This control design problem is similar to that of marine surface vessels, following position and heading, using only rudder deflection [4]. The typical approach to such guidance problems is to reduce the 2D error space by coupling the commanded course to the measured cross-track error. In this work we accomplish this by modelling the path following behavior of a 'good helmsman' [5].

Providing accurate path-following (or trajectory-tracking, which includes precision timing) are among the key engineering challenges faced to obtain full autonomy for an aerial vehicle [6]. Traditionally, path-following or trajectory-tracking control systems consist of separate guidance, navigation, and control structures. In this work the emphasis of the development is with the guidance and control elements. Ref. [7] provides relevant introductory material. In this work the aircraft capabilities are taken into account in design of the trajectories. The observation orbits require only slowly varying trajectories, hence only static performance capabilities are considered. The idea of modelling 'helmsman behavior' can be advanced by guidance design that includes consideration of maneuvering capabilities, and intuitive switching between position convergence and timing priority, as presented in [8, 9]. Similar approaches with more elaborate consideration of convergence properties are presented in [10, 11]. These approaches are amenable to feedback linearization as well as backstepping methods. Due to the nature of the observation orbits, in this work we rely on convergence to pre-specified paths. In [12] an 'approximate path following' algorithm is presented, based on a notion of convergence to within a 'tube' around the desired path, significantly reducing reliance on a-priori path information.

The path following structure will obtain a command from a path-planner (PP) algorithm [13], which provides desired waypoints with splining of straight lines and curves. The aim is to relieve the PP of the computational burden of producing 'feasible' paths. Feasibility in this case pertains to aircraft static performance constraints, possibly dependent on operating conditions.

The *Serret-Frenet* formulation from differential geometry represents a 3D path as smooth curves, which allows for convenient definition of continuous cross-track and course error. This formulation for aircraft guidance applications has the advantage of convenient parametrization of typical aircraft steady state performance, helices flown at constant speed and sideslip angle. This will also provide a convenient bases to address the effects of performance limitations. The integration of a Serret-Frenet based guidance law and a turn-coordination control innerloop leads to automatic compensation for wind. A straightforward bank-angle limit provides robustness and a means to include a-priori performance limits.

Results are demonstrated for a small UAV [14] by means of simulation of flight and sensor dynamics operating in an environmental model [15]. The emphasis in the path design is on relative position of the target with respect to the aircraft. The emphasis in the design of the guidance laws is on smooth convergence with the path parameters, using minimal heuristics. Among the immediate further work is extension of the ideas to 3D path following, and detailed analytic assessment of stability and convergence rate [16].

3. HELMSMAN BEHAVIOR BASED GUIDANCE LAW

3.1. Path Following in the Horizontal Plane

The objective of this section is to express the vector of vehicle velocity relative to the desired (2D) path in the horizontal plane, where the relative position is measured from the vehicle to the closest point on the desired path, Fig(1). If we consider a

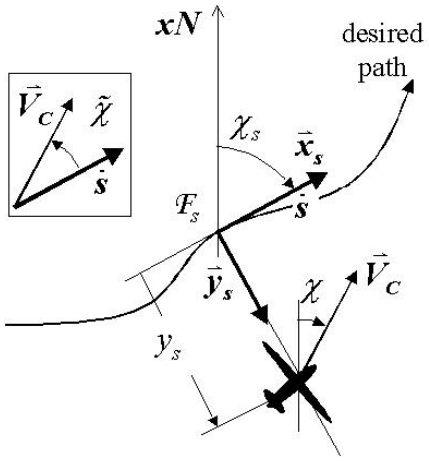

Fig. 1 The 'Serret-Frenet' frame for a 2D-path. The Serret-Frenet frame provides a means to ride along the 2D curve and illustrate its properties (curvature).

frame along the desired path $\mathcal{F}_s$, with $\mathbf{x}_s$ the unit vector in the direction of the desired inertial veloc-

ity, i.e tangential to the path, and let $\mathbf{y}_s$ be the unit normal to the path. At any point along the desired path, its curvature $\kappa(s)$ is defined as $\kappa(s) = 1/\rho(s)$ where $\rho(s)$ is the radius of the path at that point. If the direction of the path is indicated as χ_s (which is considered the desired 'course' when on the path) then the path parameters are related to yaw-rate as

$$\dot{\chi}_s(s) \;=\; \kappa(s)\dot{s}$$

and the Serret-Frenet formulas in 2D turn-coordinated flight, result in the following transformation

$$\begin{pmatrix} 1-\kappa y_s & 0 & 0 \\ 0 & 1 & 0 \\ \kappa & 0 & 1 \end{pmatrix} \begin{pmatrix} \dot{s} \\ \dot{y}_s \\ \dot{\widetilde{\chi}} \end{pmatrix} = \begin{pmatrix} c_{\widetilde{\chi}} & -s_{\widetilde{\chi}} & 0 \\ s_{\widetilde{\chi}} & c_{\widetilde{\chi}} & 0 \\ 0 & 0 & 1 \end{pmatrix} \begin{pmatrix} u_b \\ v_b \\ \dot{\chi} \end{pmatrix} \qquad (1)$$

where χ is the flown course, χ_s the trajectory direction, and the *relative course* is defined as

$$\widetilde{\chi} \;\triangleq\; \chi - \chi_s \qquad (2)$$

For coordinated level flight $u_b \approx V_C$ and $v_b = 0$. Transformation (1) is not usable when $y_s = \frac{1}{\kappa(s)} = \rho(s)$, i.e. when the vehicle is at the center of the instantaneous circle.

3.2. Guidance Law Design; Helmsman Behavior

The above expressions allow formulation of a guidance law that takes as input: inertial velocity, inertial aircraft position, and desired path to target position, and providing as output a commanded heading rate ($\dot{\chi}_{com}$). The aircraft bank-angle is the control variable.

The guidance law objective is to converge $\widetilde{\chi}$ and y_s simultaneously to zero. This may be achieved by coupling the commanded angle of convergence and cross-distance, i.e. $\widetilde{\chi}_c(y_s)$, Figure (2). According to [5], the behavior of a 'good helmsman' follows an intercept course $\widetilde{\chi}_c$ that varies with cross distance y_s, rather than using sideward velocity. This is similar to an aircraft in coordinated flight, $v_b \equiv 0$, while considering bank angle as the control variable. The helmsman behavior can be modelled as $\widetilde{\chi}_c = \chi_c - \sigma(y_s)$. Where χ_c represent the commanded absolute course, and $\sigma(y_s)$ is any function satisfying

$$\begin{aligned} y_s\sigma(y_s) &> 0 \\ \sigma(0) &= 0 \\ \sigma : y_s &\rightarrow [-\widetilde{\chi}_{icpt}, \widetilde{\chi}_{icpt}] \end{aligned}$$

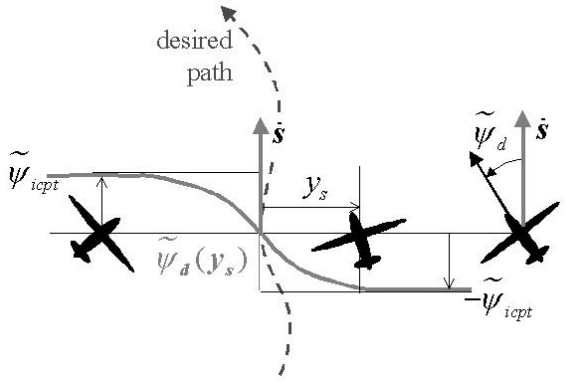

Fig. 2 The behavior of a 'good helmsman' modelled by the desired relative course $\widetilde{\chi}_d$ as function of cross-distance y_s in the form of a sigmoid function (solid line), saturating at $\pm\widetilde{\chi}_{icpt}$. $\widetilde{\chi}_c \approx 0$ when 'close' to the trajectory, and saturates at $\widetilde{\chi}_c = \pm\widetilde{\chi}_{icpt}$ when farther away.

where $\widetilde{\chi}_{icpt}$ represents the intercept angle at large cross distance. The helmsman behavior relative to a straight line course $\chi_s = 0$ is

$$\chi_c \;=\; \sigma(y_s) \qquad (3)$$

For intercepting and tracking a trajectory, the helmsman behavior is relative to the desired trajectory. The helmsman behavior is expressed by formulating the commanded course χ_c in terms of χ_s, and y_s. In that case expression (3) becomes

$$\widetilde{\chi}_c \;\triangleq\; \chi_c - \chi_s \;=\; \sigma(y_s) \qquad (4)$$

Therefore, the helmsman behavior in trajectory tracking is

$$\chi_c(y_s, \chi_s) \;=\; \sigma(y_s) + \chi_s \qquad (5)$$

Two aspects of the helmsman behavior determine the 'aggressiveness' of the intercept: the maximum intercept angle, and the 'lead-distance' or slope $d\sigma/dy_s$. One possible function is the arctan function, which allows an easy interpretation of this 'lead-distance', similar to the 'line-of-sight' guidance ideas. Another possible candidate is a sigmoidal function, figure(2), saturating at $\widetilde{\chi}_{icpt} = \pm 30^o$ for large y_s. For good path following performance it is essential to focus on these convergence properties. Heuristic course-trackers exist that obtain both efficiency and high precision, while taking advantage of maximum vehicle performance. To ensure smooth and fast convergence, the signal $\dot{\widetilde{\chi}}_c(y_s, V_C, \widetilde{\chi})$ can be determined iteratively, based on relative location, orientation, and aircraft bank performance. This is valuable for example in UAV retrieval or autoland

phase. The helmsman functions suggested in this paper generally can not obtain the same convergence performance without specific tuning. However, they are well suited for more general trajectories using a minimum of heuristics and are robust with respect to wind and turbulence.

In the following, it is assumed that the wind $\{V_w, \chi_w\}$ are known (estimated), the airspeed V_a and altitude remain approximately constant, bank angle command following performs well and fast relative to path-changes of $\pm 30^o$, and the commanded path will be mild enough to prevent extreme wind-up of path-following integral action due to roll-rate and saturation limits. The latter is a temporary assumption, hedging of the commanded heading rate will be implemented later. Let the ideal course convergence dynamics be specified as follows

$$\frac{d}{dt}\chi(t) \; = \nu(\chi, \chi_c) \tag{6}$$

where 'pseudo-control' ν refers to the 'tracking-servo' control law. Defined in terms relative to the trajectory

$$\begin{aligned} \frac{d}{dt}\{\chi - \chi_s\} &= \nu(\chi - \chi_s, \chi_c - \chi_s) \\ \Leftrightarrow \frac{d}{dt}\widetilde{\chi} &= \nu(\widetilde{\chi}, \widetilde{\chi}_c) \end{aligned} \tag{7}$$

The guidance law then is based on desired tracking dynamics by design of the pseudo control ν. In this work we consider the design:

$$\nu(\chi, \chi_c) \; \triangleq \; \dot{\chi}_c + k_p(\chi_c - \chi) + k_i \int_0^t (\chi_c - \chi)\, d\tau \tag{8}$$

in terms of the course relative to the desired path expression(7), this becomes

$$\begin{aligned} \nu(\chi - \chi_s, \chi_c - \chi_s) &= (\dot{\chi}_c - \dot{\chi}_s) + \\ & \quad k_p(\chi_c - \chi_s - \chi + \chi_s) + \\ & \quad k_i \int_0^t (\chi_c - \chi_s - \chi + \chi_s)\, d\tau \end{aligned}$$

equivalently

$$\nu(\widetilde{\chi}, \widetilde{\chi}_c) \;\; = \;\; \dot{\widetilde{\chi}}_c + k_p(\widetilde{\chi}_c - \widetilde{\chi}) + k_i \int_0^t (\widetilde{\chi}_c - \widetilde{\chi})\, d\tau$$

Herein $\widetilde{\chi}_c \; = \; \chi_c - \chi_s$ denotes the commanded relative course based on the helmsman behavior, equation(5), displayed in figure(2) and defined by

$$\sigma(y_s) \; = \; \widetilde{\chi}_{icpt} \frac{e^{-a\, y_s/2} - 1}{e^{-a\, y_s/2} + 1}$$

where $a > 0$ is a design variable such that $a\,\widetilde{\chi}_{icpt}$ represents the slope $d\sigma/dy_s$ at $y_s = 0$ (compare to a derivative gain). Therefore, the derivative signal $\dot{\chi}_c$ is constructed as

$$\begin{aligned} \dot{\chi}_c &= \frac{d}{dt}\sigma(y_s) \\ &= \sigma_{y_s}\frac{dy_s}{dt} \\ &= \sigma_{y_s} V_C \, sin(\widetilde{\chi}) \end{aligned}$$

where

$$\sigma_{y_s} \; \triangleq \; \frac{d}{dy_s}\sigma(y_s) \; = \; -a\,\widetilde{\chi}_{icpt}\, \frac{e^{-a y_s/2}}{(e^{-a y_s/2} + 1)^2}$$

The closed loop dynamics according to expression(7) then are

$$\dot{\widetilde{\chi}} \; = \; \sigma_{y_s} V_C \, sin(\widetilde{\chi}) + k_p(\widetilde{\chi}_c - \widetilde{\chi}) + k_i \int_0^t (\widetilde{\chi}_c - \widetilde{\chi})\, d\tau$$

These closed loop tracking dynamics can be interpreted as

$$\Delta\dot{\chi} + k_p\Delta\chi + k_i \int_0^t \Delta\chi\, d\tau \; = \; \Delta_{ex}$$

where $\Delta\chi \; \triangleq \; \widetilde{\chi}_c - \widetilde{\chi}$, and Δ_{ex} represents the effects of approximations and external perturbations. Formal convergence proofs can be constructed using Lyapunov-type analysis [3, 16].

In a coordinated turn, the bank angle is kinematically related to the turn rate as

$$\tan(\phi) \; = \; \frac{V_c}{g}\dot{\psi} \tag{9}$$

with the approximation $\dot{\psi} \approx \dot{\chi}$, the commanded turn rate is mapped to a commanded bank angle as

$$\phi_c \; = \; \arctan(\frac{V_c}{g}\,\nu) \tag{10}$$

The commanded bank angle is limited to $\pm 30^o$ for mild maneuvering and $\pm 45^o$ for more aggressive maneuvers. The roll rate is limited to $\pm 45^o/s$. A straightforward PI control with a 5% settling time of 3 seconds is used to construct the aileron signals.

4. PATH GEOMETRY AND KINEMATICS

4.1. Problem description

We are interested in maneuvers that allow maximum exposure of a target. We refer to the results as 'maneuvers' because they are not necessarily trimmed flight solutions. Rather, the resulting

state trajectories are defined by observation geometry and the fact that the aircraft maintains coordinated flight. It is advantageous to approach the maneuver from a pilot's perspective, and find corresponding field-of-view patterns. Thomasson [1] found analytic expressions for flight which result in a constant line-of-sight pan angle based on assumptions like level flight, no wind, small alpha, &c. In this work, we follow a similar development, and find analytical expressions for camera angles and zoom as function of yaw, yaw-rate, altitude, velocity, and wind-velocity, including the possibility of using a nonzero side slip angle [2]. Our objectives for studying the maneuvers are:

1 Analytical expressions for path parameters, as function of 'clock-angle'.
2 Feedback mechanism of path parameters in a Guidance algorithm (i.e. How does the UAV get there? How does the UAV stay there?).
3 Target exposure assessment, and required camera turret activity.
4 Minimization of heuristics in implementation.

To establish the problem of limited target exposure, we first look at a circle in wind, a.k.a. 'turn-about-a-point', i.e. given the maneuver we find the corresponding geometry. Next, we address the more interesting problem of the wind ellipse, a.k.a. 'turn-on-a-pylon' [17], where the observation geometry defines the maneuver. In the wind ellipse, the wingtip points at the target throughout the maneuver, but the aircraft maintains coordinated flight. Finally, we demonstrate the results and assess target exposure in a 'stand-off' maneuver.

4.2. Gimbal Kinematics

The camera angles required to keep the target in sight are based on aircraft pose (position and orientation) and target location. Fig 3 presents the geometry for pan, tilt, and zoom. A robust method

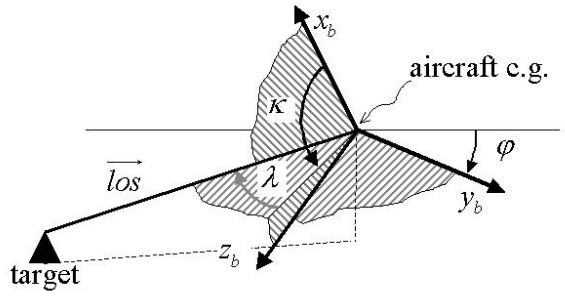

Fig. 3 Geometry for camera tilt angle κ, and pan angle λ.

of determining the gimbal angles can be achieved by using analytic expressions based on the four quadrant inverse tangent function. Using the relative position and aircraft attitude information:

1 The normalized line-of-sight is given by the relative position of aircraft and target:

$$\widehat{los}|_e \;=\; \frac{[x_{tgt}, y_{tgt}, z_{tgt}]_e^T - [x_{ac}, y_{ac}, z_{ac}]_e^T}{|[x_{tgt}, y_{tgt}, z_{tgt}]^T - [x_{ac}, y_{ac}, z_{ac}]^T|}$$

2 Find the normalized line-of-sight vector expressed in the aircraft body frame,

$$[\,\hat{x}_{los}, \hat{y}_{los}, \hat{z}_{los}\,]_b^T \;=\; {}_bT_e(\phi,\theta,\psi)\,\widehat{los}|_e$$

3 Find κ using the LOS components in the body frame as $\kappa \;=\; ATAN2(\hat{z}_{los}, \hat{x}_{los})$.
4 Find λ using the LOS components in the body frame as $\lambda \;=\; ATAN2\left(\hat{y}_{los}, \sqrt{\hat{x}_{los}^2 + \hat{z}_{los}^2}\right)$.

4.3. Camera Angle Limit Problem Demonstration

Figs(4), and(5) indicate the effect of gimbal angle saturation in a circular orbit with wind. The camera tilt angle saturates at time $t \approx 75\ s$ and onwards. To reduce the target out-of-sight problem, we wish to find the trajectory that maintains the geometry between vehicle and target constant. Two possible scenarios are considered, both assuming coordinated flight:

1 Maintaining constant tilt-angle, equivalent to maintaining a constant angle between x_b axis and line-of-sight. (e.g. keep target at two-o'-clock)
2 Maintaining both tilt- and pan-angle constant. This will require changes in altitude and/or airspeed.

An example of the second maneuver is orienting the wingtip at the target throughout the orbit. For target observation this maneuver may have the advantage of added camera stability due to the larger inertia about the x_b axis and the natural aerodynamic damping in roll.

4.4. Constant Line-of-Sight Tilt Angle

Using similar reasoning as Ref [1], but allowing for wind in arbitrary direction ψ_w, with angular position determined by 'bearing from the target' or 'clock-angle' ψ_p, and the relative position of the target measured from the x_b–axis clock-wise ζ. Hence, ζ is from the pilot's perspective, $\zeta = 60^o$ corresponds to a pilot having the target at his/her two-o'-clock position. The expression for the change in radius as a function of the relative position is:

$$\frac{dr}{d\psi_p} \;=\; r\,\frac{-V_a c_\zeta - V_w c_{\psi-\psi_w+\zeta}}{V_a s_\zeta + V_w s_{\psi-\psi_w+\zeta}} \qquad (11)$$

which can be expressed in terms of ψ_p with the relation

$$\psi_p \;=\; \zeta + \psi - \pi \qquad (12)$$

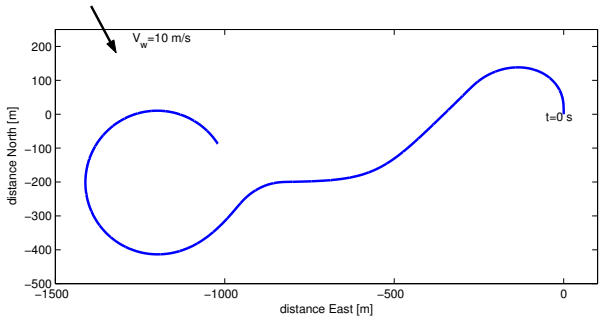

Fig. 4 Flight trajectory of 1.5 mins, with initial aircraft heading North, $V_w = 10[m/s]$, and $V_a \approx 25[m/s]$.

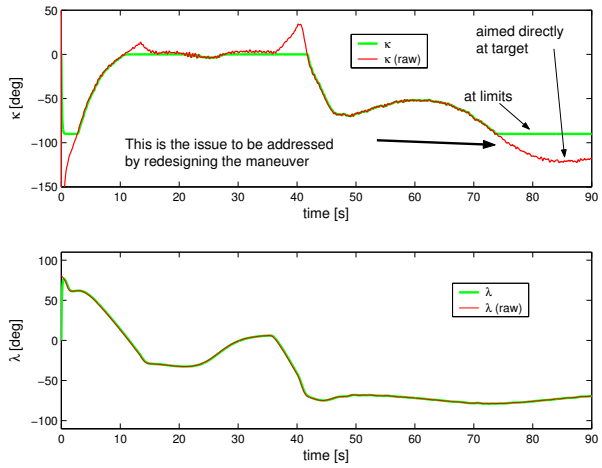

Fig. 5 Corresponding Gimbal-angles. The bank-angle requirements are reflected in the requirements on the pan-angle necessary for target capture. However, the most stringent requirements are placed on the tilt-angle capabilities. The last 20 seconds of the κ time history displays that the wind-correction requires a κ beyond the tilt-range. The effects of turbulence are also more pronounced in the κ channel (associated with pitch motion) than in the λ channel (roll).

The associated trigonometric relations

$$\begin{aligned} c_{\psi-\psi_w+\zeta} &= -c_{\psi_p}c_{\psi_w} - s_{\psi_p}s_{\psi_w} \\ s_{\psi-\psi_w+\zeta} &= c_{\psi_p}s_{\psi_w} - s_{\psi_p}c_{\psi_w} \end{aligned}$$

allow the expression:

$$\frac{dr}{d\psi_p} = r\,\frac{-V_a c_\zeta + V_w(c_{\psi_p}c_{\psi_w} + s_{\psi_p}s_{\psi_w})}{V_a s_\zeta + V_w(c_{\psi_p}s_{\psi_w} - s_{\psi_p}c_{\psi_w})} \qquad (13)$$

The special case where the target remains 'under' the wingtip throughout the maneuver, $\zeta = \frac{\pi}{2}$, can be presented as:

$$\frac{dr}{d\psi_p} = r\,\frac{V_w(c_{\psi_p}c_{\psi_w} + s_{\psi_p}s_{\psi_w})}{V_a - V_w(s_{\psi_p}c_{\psi_w} - c_{\psi_p}s_{\psi_w})} \qquad (14)$$

The radius of the orbit can be found by integration of equation(13). For $\zeta < \frac{\pi}{2}$ this requires numerical integration, for the special case $\zeta = \frac{\pi}{2}$ the result is

$$r(\psi_p) = r_0\,\frac{V_a + V_w s_{\psi_w}}{V_a - V_w s_{\psi_p-\psi_w}} \qquad (15)$$

where $r_0 = r(\psi_p = 0)$ is the radius directly North of the target. Eqn 15 represents an elliptical orbit that maintains the wingtip in the direction of, though not necessarily pointed directly at, the target. Hence, it results in a constant camera tilt-angle κ, with pan-angle depending on the vehicle bank-angle. To maintain a relative angle $\zeta < \frac{\pi}{2}$ requires a spiral trajectory towards the target, Ref [1].

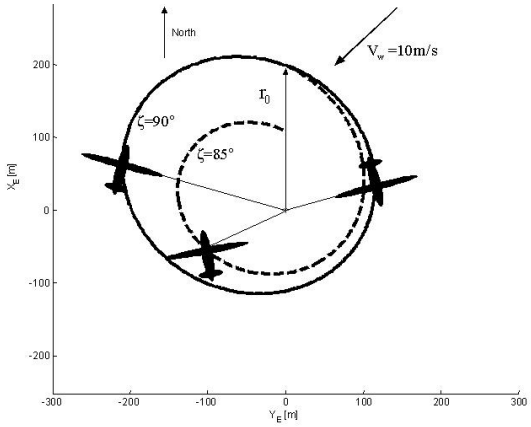

Fig. 6 Elliptical orbit for $\zeta = 90^o$, equation(15), and spiral trajectory in wind from numeric integration of equation(13) with $\zeta = 85^o$. Target at origin. $V_a = 25\ m/s$, $V_w = 10\ m/s$ from 045 deg.

The minimum radius in the elliptical orbit is related to r_0 by

$$r_{min} = r_0\,\frac{V_a + V_W}{V_a + V_W s_{\psi_W}}$$

In terms of the minimum radius, the path can be expressed as

$$r(\psi_P) = r_{min}\,\frac{V_a + V_W}{V_a - V_W s_{\psi_P-\psi_W}} \qquad (16)$$

where the minimum radius occurs at $\psi_P|_{r_{min}} = \psi_W + \pi/2$ when flying clockwise about the target. The ground speed is maximum at this point, $V_c = V_a + V_W$. Hence, given a maximum bank angle, ϕ_{max}, the minimum possible radius is

$$r_{min} = \frac{(V_a + V_W)^2}{g\,t_{\phi\,max}} \qquad (17)$$

The course in the elliptical orbit is

$$\chi(\psi_P) = \arctan\left(\frac{V_W c_{\psi_W} + V_a c_{\psi_P-\zeta}}{-V_a s_{\psi_P-\zeta} - V_W s_{\psi_W}}\right) \qquad (18)$$

From this expression, the commanded course for wingtip at target, i.e. $\zeta = \pi/2$, is constructed as

$$\chi_c(\psi_P) \;=\; \arctan\left(\frac{V_W c_{\psi_W} - V_a s_{\psi_P}}{-V_a c_{\psi_P} - V_W s_{\psi_W}}\right) \qquad (19)$$

Expressions (16), (17), and (19) can all be updated as wind speed and direction estimates become available.

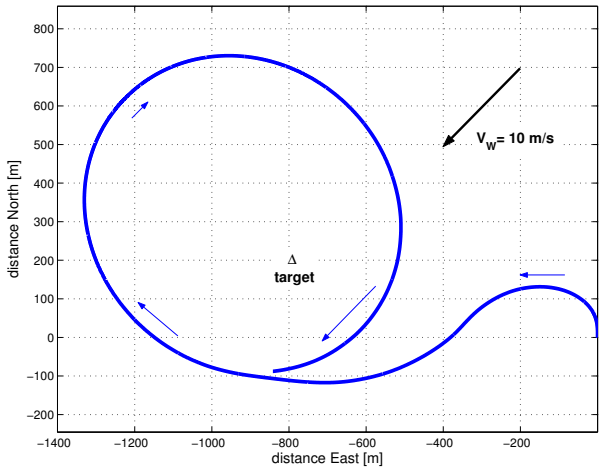

Fig. 7 Approaching the target on a course of 270^o, with wind $045^o@10m/s$. The information used to commence the orbit capture is distance to target, $d \leq 2r_0$ where $r_0 = 500\ m$ is the distance North of target. The minimum radius is related to r_0 as given by equation(17). The path parameters y_s and ψ_s are determined by equations(16), and (19).

4.5. Constant Tilt and Pan Angle

In this section we allow the altitude to change, such that we can operate the aircraft at 'pivotal altitude' [17] to maintain the wingtip on the target. A simple altitude controller is used that feeds back altitude error to the engine power setting.

4.6. Wind Estimate

The path following algorithm is independent of wind and heading information. However, the constant line-of-sight path geometry requires knowledge of local wind information. The field-of-view is robust enough to allow approximate solutions, relying on wind speed and direction estimates. Hence, the remaining objective here is to estimate the wind speed and direction.

The airspeed V_a is measured with airdata instruments, the ground speed V_C and course χ are measured by GPS, and wind speed V_w and direction ψ_w

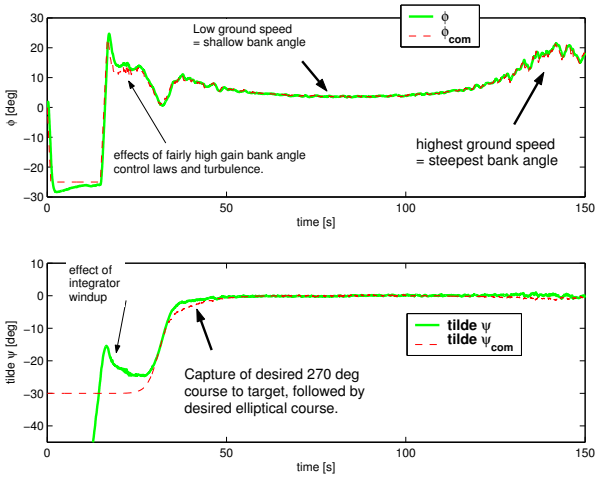

Fig. 8 Bank angle and relative course time histories corresponding to figure(7). Noise is due to Dryden moderate turbulence modeling and an aggressive bank angle control law.

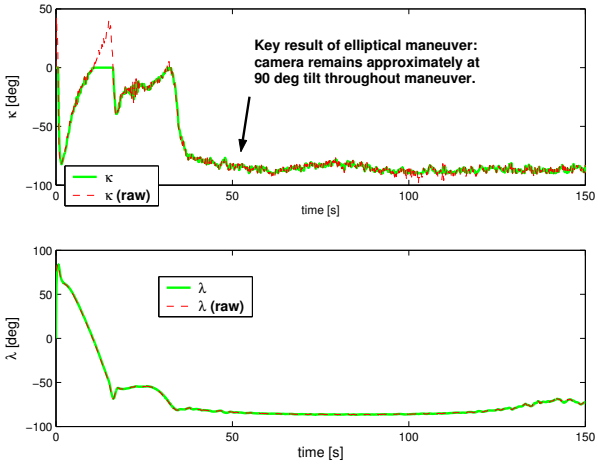

Fig. 9 Camera gimbal angles corresponding to figure(7). The key result of this maneuver is the aircraft orientation is such that the wingtip is aimed at the target throughout the maneuver.

are related to to the aircraft heading, ψ as

$$\begin{aligned} V_a &= V_c c_{\psi-\chi} - V_w c_{\psi-\psi_w} \\ 0 &= V_c s_{\psi-\chi} - V_w s_{\psi-\psi_w} \end{aligned}$$

where c_a is short hand for $\cos(a)$ &c. If the wind speed and direction are considered constant (slowly varying), then the wind speed and direction can be considered as 'unknown initial conditions' and obtained by means of an observer. In case the heading of the aircraft is not directly available the unknown aircraft heading, wind speed, and direction is an 'unobservable' problem. In that case it is still possible to find and/or update an estimate of the wind speed, direction, and aircraft heading by

an occasional course reversal maneuver and batch data processing. The following proceeds as if the aircraft heading is in fact known. In that case a nonlinear observer may be constructed to estimate the wind direction and speed. Some results are shown in Figs(15), (16), (17), and (18).

ACKNOWLEDGEMENT

This work was supported by the University of Washington, Royalty Research Fund grant 65–1914, The Insitu Group, and Hood Technology Corporation. The authors are grateful to Marius Niculescu for providing the Aerosonde dynamic model.

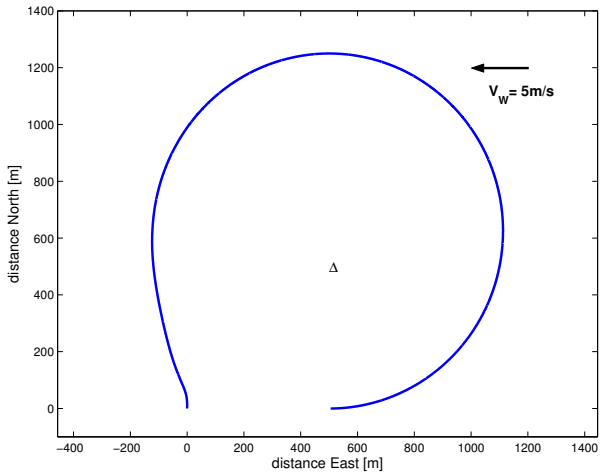

Fig. 10 'On-Pylon' maneuver; trajectory of 150 seconds of flight orbiting target at approximate pivotal altitude in light wind and turbulence. Target located at $\{North, East\} = \{500, 500\}m$, wind 090^o@5 m/s.

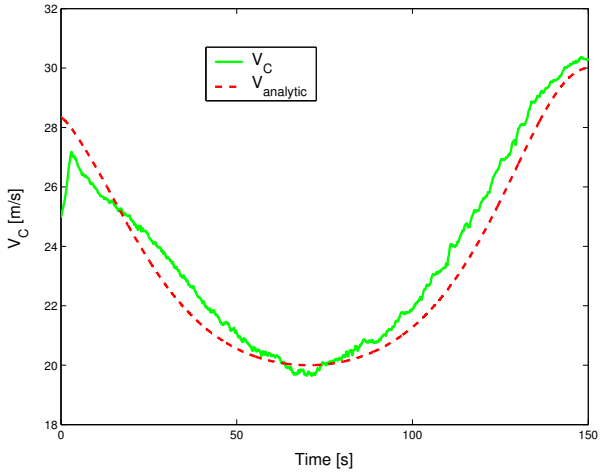

Fig. 11 Inertial speed corresponding to figure(10). $V_a \approx$ 25 m/s in turbulence.

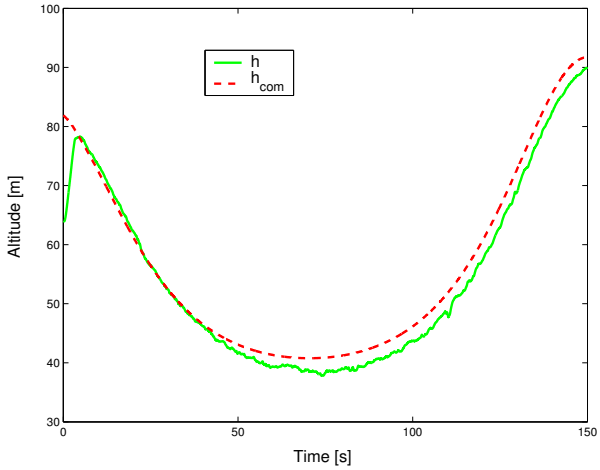

Fig. 12 'Pivotal altitude' and actual altitude time histories corresponding to figure(10). Altitude (flight path) is controlled with throttle.

REFERENCES

[1]Thomasson, "Guidance of a Roll-Only Camera for Ground Observation in Wind," *JGCD*, Vol. 21, No. 1, Jan-Feb 1998, pp. 39–44.

[2]Stolle, S. and Rysdyk, R., "Flight Path Following Guidance for Unmanned Air Vehicles with Pan-Tilt Camera for Target Observation," *22nd Digital Avionics Systems Conference*, IEEE/AIAA, Indianapolis, Indiana, October 2003.

[3]Fossen, T., Breivik, M., and Skjetne, R., "Line-of-Sight Path Following of Underactuated Marine Craft," *Proc. 6th IFAC MCMC 2003*, Girona, Spain, 2003, To appear.

[4]Skjetne, R. and Fossen, T., "Nonlinear maneuvering and control of ships," *Proc. MTS/IEEE OCEANS 2001*, IEEE, Honolulu, Hawaii, Nov. 2001, pp. 1808–1815.

[5]Pettersen, K. and Lefeber, E., "Way-point tracking control of ships," *Proc. 40th IEEE Conference on Decision and Control*, Orlando, FL, December 2001, pp. 940–945.

[6]"Unmanned Aerial Vehicles Roadmap 2002-2027," Dod memorandum, Washington, DC, December 2002.

[7]I. Kaminer, A.M. Pascoal, E. H. and Silvestre, C., "Trajectory Traking for Autonomous Vehicles: An Integrated Approach to Guidance and Control," *AIAA JGCD*, Vol. 21, No. 1, January-February 1998, pp. 29–38.

[8]Hauser, J. and Hindman, R., "Manuever Regulation from Trajectory Tracking: Feedback Linearizable Systems," *Proc. of the IFAC, Nonlinear Control System Design*, Tahoe City, CA, 1995, pp. 595–600.

[9]Hauser, J. and Hindman, R., "Aggressive Flight

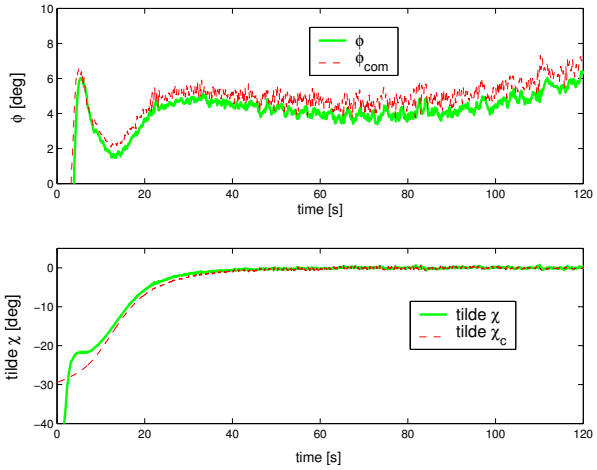

Fig. 13 Bank angle and relative course time histories corresponding to first two minutes of figure(10). Aircraft converges with exact ellipse at about $t = 30\ s$.

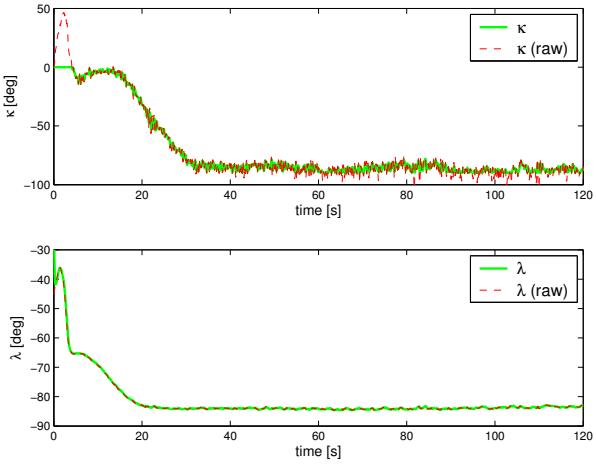

Fig. 14 Gimbal angles corresponding to first 2 min of figure(10). The purpose of this manuever is to maintain pan-angle λ near constant, while κ is also maintained near constant.

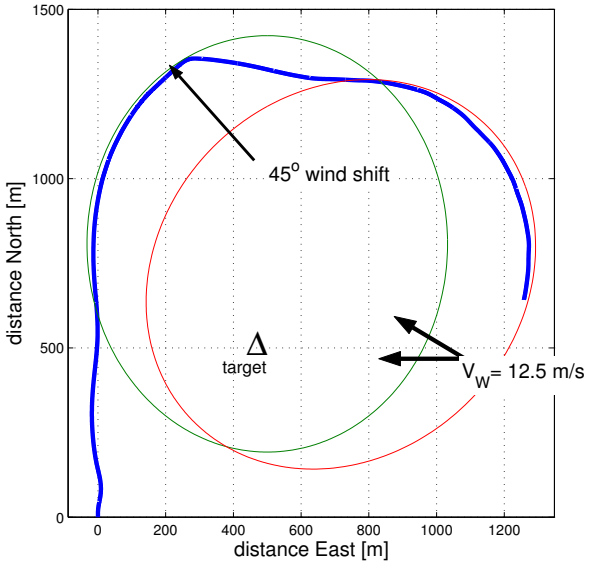

Fig. 15 Wind observation: Trace of a 3 min flight at an airspeed of $V_a = 25\ m/s$, with wind 090^o@12.5 m/s. The initial target path is an ellipse with its minimum radius $\underline{r} = 300\ m$. North-North-East of the target, the aircraft is exposed to a southerly windshift of 45^o occurring over 10 s. The new wind direction and speed is observed and subsequently used to reorient the desired path for constant observation angle.

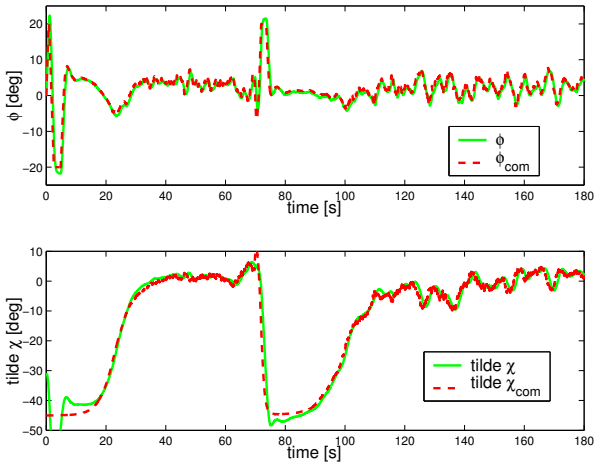

Fig. 16 Wind observation: Bank angle and relative course time histories corresponding to figure(15). The aircraft is exposed to Dryden moderate turbulence and an aggressive bank angle control law.

Maneuvers," *Proc. 36th Conference on Decision and COntrol*, San Diego, CA, December 1997, pp. 4186–4191.

[10]Skjetne, R., Fossen, T., and Kokotović, P., "Output Maneuvering for a Class of Nonlinear Systems," *Proc. 15th IFAC World Congress Automatic Control*, IFAC, Barcelona, Spain, July 2002, Accepted for publication in IFAC Automatica.

[11]Breivik, M., *Nonlinear Maneuvering Control of Underactuated Ships*, Msc thesis report, Norwegian university of Science and Technology, Dept. of Engineering Cybernetics, June 2003.

[12]Aicardi, M., Casaline, G., Indiveri, G., Aguiar, A., Encarnacao, P., and Pascoal, A., "A Planar Path Following Controller for Underactuated Marine Ve-

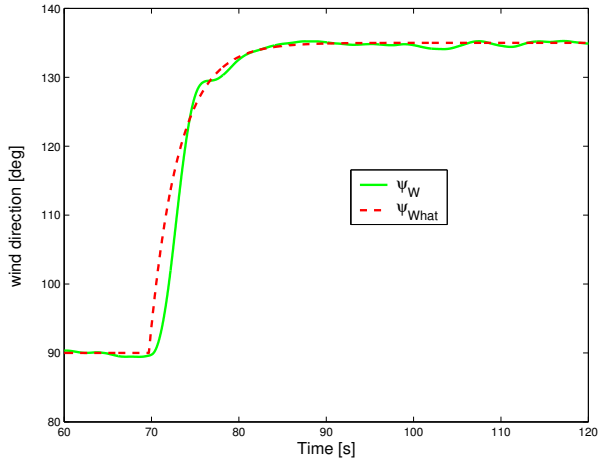

Fig. 17 Wind observation performance; estimation of wind direction $\widehat{\psi}_W$ corresponding to the second minute of flight in figure(15). The aircraft experiences a windshift from $\psi_W = 90^o$ to $\psi_W = 135^o$.

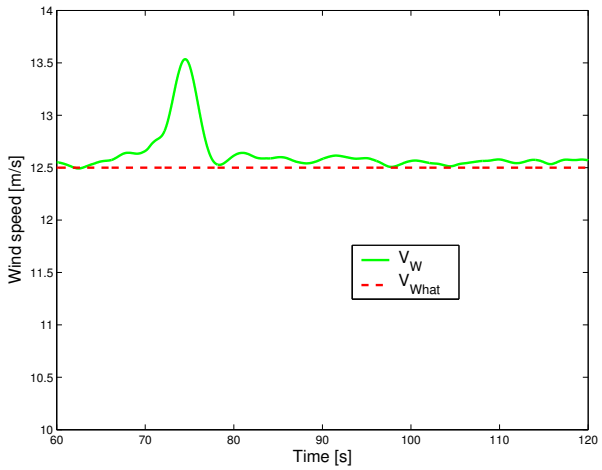

Fig. 18 Wind observation performance; estimation of wind speed $\widehat{V}_W$ corresponding to the second minute of flight in figure(15). The wind speed is constant at $V_W = 12.5\ m/s$.

hicles," *IEEE MED01*, Dubrovnik, Croatia, June 2001.

[13]Rathbun, D., Kragelund, S., Pongpunwattana, A., and Capozzi, B., "An Evolution Based Path Planning Algorithm for Autonomous Motion of a UAV Through Uncertain Environments," *Digital Avionics Systems Conference*, 2002.

[14]"Aerosonde," web-site, The Insitu Group Inc., http://www.insitugroup.net/Pages/aerosonde.html.

[15]"Dynamic Model of Aerosonde UAV," web-site, Unmanned Dynamics LLC., http://www.u-dynamics.com/aerosim/.

[16]*3D Path Following for Autonomous Underwater Vehicle*, Proc. 39th IEEE CDC, Sydney, Australia, December 2000, pp.2977-2982.

[17]Denker, J. S., *See How It Flies, Section 16.14*, http://www.av8n.com/how/htm/maneuver.html.